Enhanced OFDM-Based Optical Spatial Modulation

Chen Chen^{1,*}, Xin Zhong¹, Shu Fu¹, Xin Jian¹, Min Liu¹, Xiong Deng², and Hongyan Fu³
¹School of Microelectronics and Communication Engineering, Chongqing University, China
²Department of Electrical Engineering, Eindhoven University of Technology (TU/e), Netherlands
³Tsinghua-Berkeley Shenzhen Institute (TBSI), Tsinghua University, Shenzhen 518055, China
^{*}c.chen@cqu.edu.cn

Abstract-Optical spatial modulation (OSM) and orthogonal frequency division multiplexing (OFDM) are two promising techniques for bandlimited intensity modulation/direct detection (IM/DD) optical wireless communication (OWC) systems. In this paper, we for the first time propose a novel enhanced OFDMbased OSM scheme for spectral efficiency improvement of bandlimited IM/DD OWC systems. The proposed enhanced OFDMbased OSM scheme can be considered as the combination of timedomain OSM (TD-OSM) and non-Hermitian symmetry OFDM (NHS-OFDM). In an OWC system adopting enhanced OFDMbased OSM, a pair of light-emitting diode (LED) transmitters are selected from the LED array, which are used to separately transmit the real and imaginary parts of a complex-valued NHS-OFDM signal. A modified maximum-likelihood (ML) detector is further developed to efficiently estimate the indexes of the LED pair and the real and imaginary parts of the transmitted complexvalued NHS-OFDM signal. We show that the proposed enhanced OFDM-based OSM scheme can achieve substantially improved spectral efficiency with moderate inter-channel interference and low transceiver complexity. Simulation results clearly verify the superiority of the proposed enhanced OFDM-based OSM scheme over the existing OFDM-based OSM schemes.

Index Terms—Optical wireless communication (OWC), optical spatial modulation (OSM), orthogonal frequency division multiplexing (OFDM), multiple-input multiple-output (MIMO).

I. Introduction

Recently, there has been a rapid growth of smart mobile devices in our daily life, due to the increased requirement of emerging services such as high definition video streaming, low-latency gaming, virtual/augmented reality and Internet-of-things. In order to meet the demand for these data-greedy services, there will be an exponential increase of the mobile data traffic in the near future. Considering that the existing radio frequency (RF) spectrum will be saturated soon, the optical spectrum (including visible light, infrared and ultraviolet) reals great potential to support the ever-increasing mobile data traffic [1]. Lately, optical wireless communication (OWC) has been attracting great interest in both academia and industry due to its inherent ability to meet the demand of heavy data traffic [2], [3].

Typical OWC systems usually utilize light-emitting diodes (LEDs) or laser diodes (LDs) as transmitters and photo-diodes

This work was supported by the National Natural Science Foundation of China under Grant 61901065.

(PDs) as receivers. Moreover, intensity modulation with direct detection (IM/DD) is generally adopted for signal transmission in OWC systems. Therefore, only real-valued and non-negative signals can be successfully transmitted [4]. Although OWC systems exhibit many advantages, the achievable modulation bandwidth of commercial off-the-shelf optical elements is relatively small, especially for white LEDs which usually have a 3-dB bandwidth of about several MHz [5]. In order to enhance the capacity of OWC systems given a limited modulation bandwidth, the overall system spectral efficiency should be substantially enhanced.

To date, many techniques have been proposed for spectral efficiency enhancement of bandlimited IM/DD OWC systems. Particularly, orthogonal frequency division multiplexing (OFDM) modulation and optical multiple-input multipleoutput (MIMO) transmission have shown to be two effective techniques that have been widely investigated in OWC systems [6]-[8]. For OFDM modulation, high-order quadrature amplitude modulation (QAM) constellations can be applied to improve the spectral efficiency. Nevertheless, due to the IM/DD nature of OWC systems, conventional complex-valued OFDM signals cannot be directly transmitted in OWC systems. To obtain a real-valued and non-negative OFDM signal for intensity modulation, the Hermitian symmetry constraint is usually imposed and a direct current (DC) bias is usually added to convert the bipolar OFDM signal into a unipolar one [9]-[11]. However, the imposing of the Hermitian symmetry constraint in OFDM modulation inevitably halves its achievable spectral efficiency. For optical MIMO transmission, several schemes have been considered for OWC systems, such as spatial diversity, spatial multiplexing and spatial modulation [7]. Particularly, optical spatial modulation (OSM) has been attracted intense attention lately, due to its inherent advantages of negligible inter-channel interference (ICI), high power efficiency and low transceiver complexity [12], [13].

The combination of OFDM modulation and SM has been further proposed as a promising candidate for efficient spectral efficiency enhancement in bandlimited IM/DD OWC systems. In [14], [15], frequency-domain OSM (FD-OSM) was investigated, where SM was implemented in the frequency domain before OFDM modulation. In FD-OSM, all the transmitters are activated to transmit different time-domain samples at each

time instant, and thus FD-OSM suffers from severe ICI which cannot fully benefit from the inherent advantages of original OSM. Moreover, the transceiver complexity of FD-OSM is high since it requires multiple OFDM modulator/demodulator pairs. In [16]-[18], time-domain OSM (TD-OSM) was further proposed, where SM was realized in the time domain after OFDM modulation and a secondary DC bias was added so as to avoid any zero-value time-domain samples. Compared with FD-OSM, TD-OSM has completely eliminated ICI because only a single transmitter is activated at each time instant. In addition, the transceiver complexity of TD-OSM is much reduced since only a single OFDM modulator/demodulator pair is required. It has been shown that the spectral efficiency contributed by constellation symbols is the same for both FD-OSM and TD-OSM. In contrast, a doubled spectral efficiency contributed by spatial symbols can be achieved by TD-OSM in comparison to FD-OSM, which is due to the fact that the encoding of spatial symbols in TD-OSM is performed in the time domain. Nevertheless, the Hermitian symmetry constraint is still imposed in OFDM-based TD-OSM, which might be another key factor that can be considered to further enhance the achievable spectral efficiency of OWC systems.

In this paper, we for the first time propose and investigate a novel enhanced OFDM-based OSM scheme to substantially improve the spectral efficiency of bandlimited IM/DD OWC systems. By replacing Hermitian symmetry-based OFDM (HS-OFDM) with non-Hermitian symmetry OFDM (NHS-OFDM) in TD-OSM, the Hermitian symmetry constraint is removed. By transmitting the real and imaginary parts of the complex-valued NHS-OFDM signal via a pair of LEDs in TD-OSM, the overall spectral efficiency of the OWC systems can be significantly enhanced. The main contributions of this work can be summarized as follows:

- An enhanced OFDM-based OSM scheme combining TD-OSM with NHS-OFDM modulation is for the first time proposed for bandlimited IM/DD OWC systems, which enjoys the advantages of substantially improved spectral efficiency, moderate ICI and low transceiver complexity.
- A modified maximum-likelihood (ML) detection algorithm is designed for efficient estimation of the indexes of the LED pair, as well as the real and imaginary parts of the transmitted complex-valued NHS-OFDM signal.
- Simulation results are presented to verify the superiority
 of the proposed enhanced OFDM-based OSM scheme
 over conventional FD-OSM and TD-OSM in a typical
 indoor environment. The impact of the added secondary
 DC bias on the bit error rate (BER) performance of TDOSM and enhanced TD-OSM is also analyzed.

The rest of this paper is organized as follows. In Section II, we first introduce the principle of NHS-OFDM and the MIMO-OWC channel model, and then we discuss our newly proposed enhanced OSM scheme using NHS-OFDM. Detailed simulation setup and results are presented in Section III. Finally, Section IV concludes the paper.

Notation: $(\cdot)^T$, $(\cdot)^*$ and $(\cdot)^{\dagger}$ represent the transpose, con-

jugated transpose and pseudo inverse of a vector or matrix, respectively. $(\cdot)^{-1}$ denotes the inverse of a matrix.

II. SYSTEM MODEL

In this section, the basic principle of NHS-OFDM and the MIMO-OWC channel model are first introduced, and then an enhanced OSM scheme using NHS-OFDM is proposed and described in detail.

A. NHS-OFDM

The NHS-OFDM scheme was originally proposed for performance improvement of spatial multiplexing-based MIMO-OWC systems [19], [20]. In NHS-OFDM, the Hermitian symmetry constraint, which is generally required in HS-OFDM so as to obtain a real-valued OFDM signal [9], can be removed by separately transmitting the real and imaginary parts of the complex-valued signal via a pair of LEDs.

For a N-point IFFT, totally N-2 subcarriers can be utilized to transmit valid data. As a result, the input vector of IFFT is given by

$$\mathbf{X} = [0, X_1, \cdots, X_{N/2-1}, 0, X_{N/2+1}, \cdots, X_{N-1}]^T, \quad (1)$$

and the complex-valued time-domain signal at the output of IFFT can be represented by

$$x_m = \frac{1}{\sqrt{N}} \sum_{k=0}^{N-1} X_k \exp\left(\frac{j2\pi km}{N}\right). \tag{2}$$

In order to obtain real-valued time-domain samples, the real and imaginary parts of x_m , i.e., $x_{\mathrm{Re},m}$ and $x_{\mathrm{Im},m}$, are extracted. When N is large enough, $x_{\mathrm{Re},m}$ and $x_{\mathrm{Im},m}$ can be assumed to follow zero-mean Gaussian distributions with variances σ_{Re}^2 and σ_{Im}^2 , respectively. Similarly, the biased and clipped real and imaginary parts can be obtained as follows:

$$s_{\text{Re},m} = \begin{cases} 0, & x_{\text{Re},m} < -b_{\text{Re}} \\ x_{\text{Re},m} + b_{\text{Re}}, & x_{\text{Re},m} \ge -b_{\text{Re}} \end{cases},$$
(3)

$$s_{\text{Im},m} = \begin{cases} 0, & x_{\text{Im},m} < -b_{\text{Im}} \\ x_{\text{Im},m} + b_{\text{Im}}, & x_{\text{Im},m} \ge -b_{\text{Im}} \end{cases}, \tag{4}$$

where $b_{\rm Re} = \alpha \sigma_{\rm Re}$ and $b_{\rm Im} = \alpha \sigma_{\rm Im}$ are the corresponding DC biases added to the real and imaginary parts of $x_{\rm NHS,m}$, respectively. The DC bias in decibels is defined as $b_{dB} = 10\log_{10}(\alpha^2 + 1)$ with α being the proportionality constant.

At the receiver side, the transmitted real and imaginary parts (i.e., $x_{\mathrm{Re},m}$ and $x_{\mathrm{Im},m}$) can be separately estimated. Let $\hat{x}_{\mathrm{Re},m}$ and $\hat{x}_{\mathrm{Im},m}$ denote the recovered real and imaginary parts, respectively. The transmitted complex-valued time-domain signal $x_{\mathrm{NHS},m}$ can be estimated by

$$\hat{x}_{\text{NHS},m} = \hat{x}_{\text{Re},m} + j\hat{x}_{\text{Im},m}.$$
 (5)

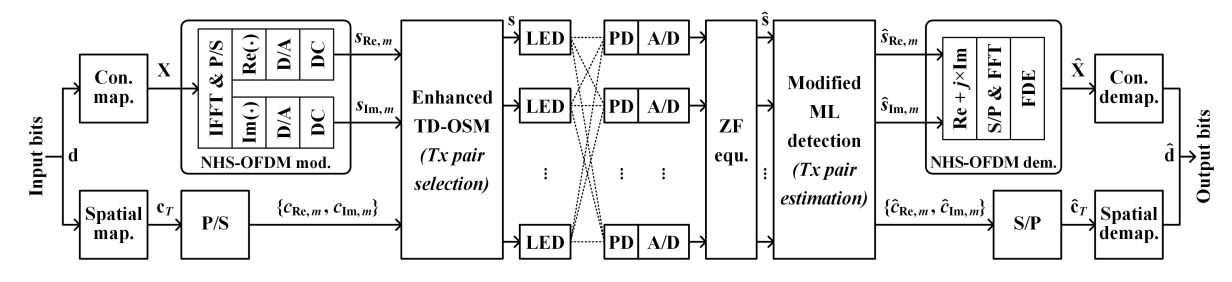


Fig. 1. Schematic diagram of the proposed enhanced TD-OSM (eTD-OSM) using NHS-OFDM. Con.: constellation; map.: mapping; mod.: modulation; equ.: equalization; dem.: demodulation; demapping.

B. MIMO-OWC Channel Model

In the following analysis, we consider a general IM/DD-based MIMO-OWC system equipped with N_t LEDs and N_r PDs. Let $\mathbf{s} = [s_1, s_2, \cdots, s_{N_t}]^T$ be the transmitted signal vector, \mathbf{H} represent the $N_r \times N_t$ MIMO channel matrix and $\mathbf{n} = [n_1, n_2, \cdots, n_{N_r}]^T$ denote the additive noise vector. The received signal vector $\mathbf{y} = [y_1, y_2, \cdots, y_{N_r}]^T$ can be given by

$$y = Hs + n. (6)$$

The DC channel gain between the r-th PD and the t-th LED, i.e., the element in the r-th row and the t-th column of \mathbf{H} , can be calculated by

$$h_{rt} = \frac{(l+1)\rho A}{2\pi d_{rt}^2} \cos^m(\varphi_{rt}) T_s(\theta_{rt}) g(\theta_{rt}) \cos(\theta_{rt}), \quad (7)$$

where $l=-\ln 2/\ln(\cos(\Psi))$ is the Lambertian emission order and Ψ denotes the semi-angle at half power of the LED; ρ and A are the responsivity and the active area of the PD, respectively; d_{rt} is the distance between the r-th PD and the t-th LED; φ_{rt} and θ_{rt} are the emission angle and the incident angle, respectively; $T_s(\theta_{rt})$ is the gain of optical filter; $g(\theta_{rt})=\frac{n^2}{\sin^2\Phi}$ is the gain of optical lens, where n and Φ are the refractive index and the half-angle field-of-view (FOV) of the optical lens, respectively.

To recover the transmitted signal vector **x**, zero forcing (ZF)-based MIMO de-multiplexing is adopted [21], [22]. After applying ZF-based MIMO de-multiplexing, the estimate of **s** can be obtained as follows:

$$\hat{\mathbf{s}} = \mathbf{H}^{\dagger} \mathbf{y} = \mathbf{s} + \mathbf{H}^{\dagger} \mathbf{n},\tag{8}$$

where $\mathbf{H}^{\dagger} = (\mathbf{H}^*\mathbf{H})^{-1}\mathbf{H}^*$ is the pseudo inverse of \mathbf{H} .

The additive noise usually consists of both shot and thermal noises, which can be reasonably modeled as a real-valued zero-mean additive white Gaussian noise (AWGN) with power $P_n = N_0 B$, where N_0 and B denote the noise power spectral density (PSD) and the modulation bandwidth, respectively.

C. Enhanced OSM Using NHS-OFDM

In order to substantially improve the spectral efficiency of IM/DD-based MIMO-OWC systems while averting severe ICI

and high transceiver complexity, we propose and investigate a novel enhanced OSM scheme in this work. The proposed enhanced OSM scheme can be considered as the combination of TD-OSM with NHS-OFDM modulation.

The schematic diagram of the proposed enhanced TD-OSM (eTD-OSM) scheme using NHS-OFDM modulation is shown in Fig. 1. As we can see, the input vector of bits **d** is first mapped to a constellation vector \mathbf{X} as defined by (1) and a spatial vector $\mathbf{c}_T = [c_0, c_1, \cdots, c_{N-1}]^T$. The constellation vector X is fed into a NHS-OFDM modulator which generates two outputs, i.e., $s_{\text{Re},m}$ and $s_{\text{Im},m}$, for $m \in \{0, 1, \dots, N-1\}$. Differing from conventional TD-OSM using HS-OFDM which only selects a single LED to transmit the constellation symbols, the proposed enhanced TD-OSM selects a pair of LEDs to separately transmit $s_{Re,m}$ and $s_{Im,m}$. Let $c_{Re,m}$ and $c_{Im,m}$ denote the indexes of the selected two LEDs to transmit $s_{Re,m}$ and $s_{\text{Im},m}$, respectively. More specifically, here we assume that $c_{\text{Re},m} < c_{\text{Im},m}$, i.e., $s_{\text{Re},m}$ is transmitted by the LED which has a smaller index in the selected LED pair while $s_{{
m Im},m}$ is transmitted by the LED with a larger index.

For the MIMO-OWC system with N_t LED transmitters, the number of combinations to select two out of N_t LEDs is obtained by $C(N_t,2)$, where $C(\cdot,\cdot)$ denotes the binomial coefficient. As a result, the spectral efficiency (bits/s/Hz) of the proposed enhanced TD-OSM using NHS-OFDM with N_t LED transmitters and M-ary constellation is calculated by

$$\eta_{\text{eTD-SM}} = \underbrace{\log_2(M)}_{\text{constellation}} + \underbrace{\lfloor \log_2(C(N_t, 2)) \rfloor}_{\text{spatial}}.$$
(9)

For the purpose of comparison, the spectral efficiencies of conventional FD-OSM and TD-OSM using HS-OFDM are given as follows [17], [18]:

$$\eta_{\text{FD-OSM}} = \underbrace{\frac{1}{2} \log_2(M)}_{\text{constellation}} + \underbrace{\frac{1}{2} \lfloor \log_2(N_t) \rfloor}_{\text{spatial}},$$
(10)

$$\eta_{\text{TD-OSM}} = \underbrace{\frac{1}{2} \log_2(M)}_{\text{contribution}} + \underbrace{\lfloor \log_2(N_t) \rfloor}_{\text{spatial}}.$$
 (11)

Compared with conventional FD-OSM and TD-OSM using HS-OFDM, we can see that the scaling factor $\frac{1}{2}$ corresponding to the spectral efficiency contributed by constellation symbols

is eliminated in the proposed enhanced TD-OSM using NHS-OFDM, which is basically due to the removal of the Hermitian symmetry constraint in NHS-OFDM. Moreover, the spectral efficiency contributed by spatial symbols in enhanced TD-OSM is increased from $\lfloor \log_2(N_t) \rfloor$ to $\lfloor \log_2(C(N_t,2)) \rfloor$ in comparison to conventional TD-OSM using HS-OFDM.

After LED pair selection, a pair of LEDs are activated to transmit the real and imaginary part of a complex-valued signal at each time instant. Therefore, the transmitted signal vector $\mathbf{s} = [s_1, s_2, \cdots, s_{N_t}]^T$ can be generated. At the receiver side, after applying ZF equalization as given by (8), the recovered signal vector can be obtained by $\hat{\mathbf{s}} = [\hat{s}_1, \hat{s}_2, \cdots, \hat{s}_{N_t}]^T$. Subsequently, a modified ML detector is employed to identify the indexes of the selected two LEDs and estimate the real and imaginary parts of the transmitted complex-valued signal.

Algorithm 1 Modified ML detection for enhanced TD-OSM using NHS-OFDM

```
Input: \hat{\mathbf{s}} = [\hat{s}_1, \hat{s}_2, \cdots, \hat{s}_{N_t}]^T
Output: \hat{s}_{\text{Re},m}, \hat{s}_{\text{Im},m}, \{\hat{c}_{\text{Re},m}, \hat{c}_{\text{Im},m}\}
for m=0 to N-1 do

Sort the elements of \hat{\mathbf{s}} in the descending order
Obtain the sorted index vector \mathbf{i} = [i_1, i_2, \cdots, i_{N_t}]^T
Abstract \mathbf{i}' = [i_1, i_2]^T
Sort the elements of \mathbf{i}' in the ascending order
Obtain the sorted index vector \mathbf{c} = [c_1, c_2]^T
Obtain \hat{s}_{\text{Re},m} = \hat{s}_{c_1}, \hat{s}_{\text{Im},m} = \hat{s}_{c_2}
Obtain \{\hat{c}_{\text{Re},m}, \hat{c}_{\text{Im},m}\} = \{c_1, c_2\}
end for
```

The detailed procedures of the modified ML detection are presented in Algorithm 1. The recovered signal vector \$\hat{\mathbf{s}}\$ is treated as the input and its elements are first sorted in the descending order so as to achieve the sorted index vector $\mathbf{i} = [i_1, i_2, \cdots, i_{N_t}]^T$. Then, the first two elements of \mathbf{i} are abstracted and an index vector $\mathbf{i}' = [i_1, i_2]^T$ is obtained. After that, the elements of i' are further sorted in the ascending order to get the sorted index vector $\mathbf{c} = [c_1, c_2]^T$. Consequently, the estimated real and imaginary parts of the transmitted complexvalued signal can be obtained by $\hat{s}_{\text{Re},m} = \hat{s}_{c_1}$ and $\hat{s}_{\text{Im},m} = \hat{s}_{c_2}$, respectively. Moreover, the combination of the indexes of the two selected LEDs can also be obtained by $\{\hat{c}_{Re,m},\hat{c}_{Im,m}\}=$ $\{c_1, c_2\}$. Given the estimated $\hat{s}_{Re,m}$ and $\hat{s}_{Im,m}$, the transmitted complex-valued signal can be recovered by using (5), which is further fed into a NHS-OFDM demodulator to obtain the estimate of the transmitted constellation vector \mathbf{X} , i.e., $\hat{\mathbf{X}}$. The estimate of the transmitted spatial vector \mathbf{c}_T , i.e., $\hat{\mathbf{c}}_T$, can also be obtained via serial-to-parallel (S/P) convention. Finally, the output vector of bits **d** are generated after constellation demapping and spatial demapping.

As we can observed from Fig. 1, the ICI in the proposed enhanced OFDM-based OSM scheme is moderate, since only a pair of LEDs are activated to transmit different time-domain samples, which is substantially lower than that of FD-OSM and slightly higher than that of TD-OSM when the number of LEDs is relatively large. Furthermore, the transceiver com-

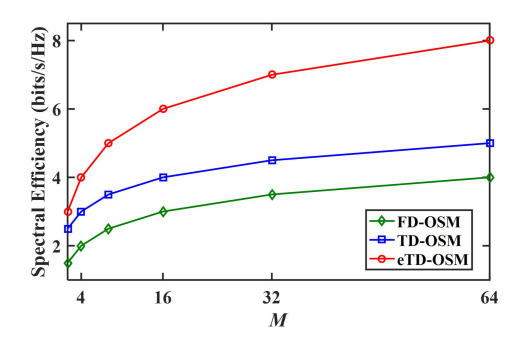


Fig. 2. Spectral efficiency vs. M for FD-OSM, TD-OSM and enhanced TD-OSM (eTD-OSM) with $N_t = 4$.

plexity of the proposed enhanced OFDM-based OSM scheme is relatively low, due to the fact that only a single pair of NHS-OFDM modulator/demodulator is needed.

III. SIMULATION RESULTS

In this section, we evaluate and compare the performance of conventional FD-OSM and TD-OSM using HS-OFDM and the proposed enhanced TD-OSM using NHS-OFDM in typical indoor MIMO-OWC systems through numerical simulations.

A. Simulation Setup

In our simulations, we consider a 4×4 MIMO-OWC system in a typical indoor environment with a dimension of 5 m \times 5 m \times 3 m. The 2×2 LED array is located at the center of the ceiling and the spacing between two adjacent LEDs is 2.5 m. The user equipped with a 2×2 PD array is located at (2 m, 2 m, 0.85 m) over the receiving plane, which is 0.85 m above the floor, and the spacing between two adjacent PDs is 10 cm. The LEDs are oriented downwards to point straight to the receiving plane and the PDs are vertically oriented towards the ceiling. The semi-angle at half power of each LED is 60° . The gain of the optical filter is 0.9. The refractive index and the half-angle FOV of the optical lens are 1.5 and 72° , respectively. Each PD has a responsivity of 1~A/W and an active area of $1~\text{cm}^2$. The modulation bandwidth is set to 20 MHz and the noise PSD is $10^{-22}~\text{A}^2/\text{Hz}$.

B. Spectral Efficiency

We first investigate the spectral efficiency of conventional FD-OSM and TD-OSM using HS-OFDM and the proposed enhanced TD-OSM using NHS-OFDM in the MIMO-OWC system with N_t LED transmitters and M-ary constellation. Fig. 2 shows the spectral efficiency versus constellation order M for FD-OSM, TD-OSM and enhanced TD-OSM with N_t = 4. As we can see, a much smaller constellation order is required to achieve the same spectral efficiency as conventional FD-OSM and TD-OSM when applying the proposed enhanced TD-OSM. More specifically, the required constellation orders for FD-OSM, TD-OSM and enhanced TD-OSM to achieve the same spectral efficiency of 4 bits/s/Hz are 64, 16 and 4, respectively.

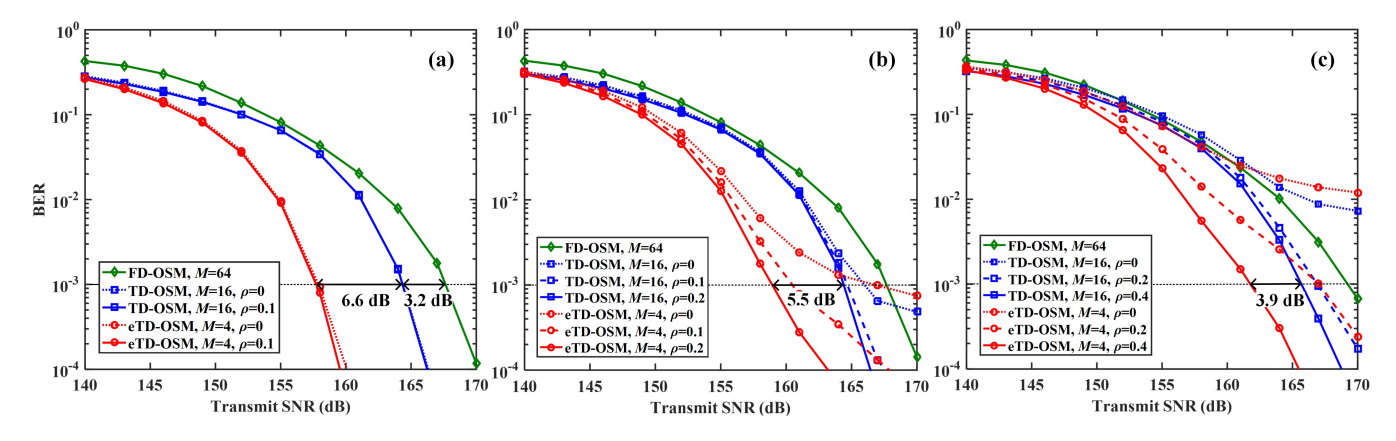


Fig. 3. BER vs. transmit SNR for FD-OSM, TD-OSM and enhanced TD-OSM (eTD-OSM) with (a) $b_{\rm dB}$ = 13 dB, (b) $b_{\rm dB}$ = 10 dB, and (c) $b_{\rm dB}$ = 7 dB.

C. BER Performance

We further compare the BER performance of conventional FD-OSM and TD-OSM using HS-OFDM and the proposed enhanced TD-OSM using NHS-OFDM. In a typical indoor MIMO-OWC system, the channel gain, as defined by (7), might be different for different LED/PD pairs due to the specific distance and emission/incident angle of each LED/PD pair. As a result, the received signal-to-noise ratios (SNRs) corresponding to different LED/PD pairs might not always be the same. To ensure a fair performance comparison of different OFDM-based OSM schemes under different MIMO settings in the indoor OWC system, we evaluate the BER performance with respect to the transmit SNR [7].

Fig. 3(a) shows the BER performance versus transmit SNR for FD-OSM, TD-OSM and enhanced TD-OSM (eTD-OSM) with a DC bias of $b_{dB} = 13$ dB. As discussed in Section III.B, the constellation orders are set to 64, 16 and 4 for FD-OSM, TD-OSM and enhanced TD-OSM to achieve a spectral efficiency of 4 bits/s/Hz. Moreover, for both TD-OSM and enhanced TD-OSM, two secondary DC biases values with the ratio of $\rho = 0$ and 0.1 are considered. It can be seen that FD-OSM requires a transmit SNR of 167.6 dB to achieve a BER of 10^{-3} . For TD-OSM, nearly the same BER can be obtained when $\rho = 0$ and 0.1, which is because a relatively large 13-dB DC bias is added and the number of zeros in the time-domain samples is negligible. The required transmit SNR for TD-OSM to achieve a BER of 10⁻³ is 164.2 dB and hence a 3.2-dB SNR improvement is attained by TD-OSM compared with FD-OSM. For enhanced TD-OSM, the BER performance is also comparable when $\rho = 0$ and 0.1, due to the use of a relatively large DC bias. It is worth noticing that a significant 6.6-dB SNR gain to achieve a BER of 10^{-3} can be obtained by enhanced TD-OSM in comparison to conventional TD-OSM. When the added DC bias is reduced to $b_{\rm dB}$ = 10 dB, as shown in Fig. 3(b), the number of zeros in the time-domain samples becomes non-negligible. Hence, the BER performance of TD-OSM with $\rho = 0$ is dominated by the errors of spatial demapping due to the existence of increasing zeros in the time-domain samples. It can be found that the

BER performance of TD-OSM can be greatly improved when $\rho = 0.1$ and further increasing ρ to 0.2 leads to marginal BER improvement, indicating that a secondary DC bias with ρ = 0.1 can efficiently reduce the number of zeros in the timedomain samples. It can also be observed that enhanced TD-OSM performs worse than conventional TD-OSM in the high SNR region when $\rho = 0$, suggesting that enhanced TD-OSM is more sensitive to the existence of zeros in the time-domain samples. Furthermore, the BER performance of enhanced TD-OSM can be gradually improved when ρ is increased to 0.1 and 0.2. More specifically, a 5.5-dB SNR improvement at a BER of 10^{-3} can be achieved by enhanced TD-OSM over conventional TD-OSM. By further reducing the added DC bias to $b_{dB} = 7$ dB, we can observe that error floors might occur for both TD-OSM and enhanced TD-OSM when $\rho = 0$, due to high spatial errors caused by a large number of zeros in the timedomain samples. In addition, the use of a larger secondary DC bias can substantially reduce the spatial errors and improve the overall BER performance, especially for enhanced TD-OSM. When $\rho = 0.4$, enhanced TD-OSM achieves an SNR gain of 3.9 dB at a BER of 10^{-3} compared with TD-OSM.

D. Impact of Secondary DC Bias

Finally, we analyze the impact of the added secondary DC bias on the BER performance of TD-OSM and enhanced TD-OSM. Fig. 4 presents the BER versus the ratio between the secondary DC bias and the primary DC bias, i.e., ρ , for different primary DC bias levels with $N_t = 4$ and a transmit SNR of 165 dB, where the achieved spectral efficiency is 4 bits/s/Hz. As we can observe, for a DC bias of $b_{\rm dB}$ = 13 dB, TD-OSM achieves a stable BER of about 5.6×10^{-4} when ρ is in the range from 0 to 0.5. It indicates that the adverse effect of zeros in the time-domain samples is negligible. However, the BER of enhanced TD-OSM can be reduced from 9.8×10^{-6} to 1.5×10^{-6} when ρ is increased from 0 to 0.1 with $b_{\rm dB} = 13$ dB. With the decrease of b_{dB} to 10 dB, TD-OSM and enhanced TD-OSM have nearly the same BER of about 10^{-3} when ρ = 0. Further increasing ρ can only slightly reduce the BER of TD-OSM and an error of about 6×10^{-4} occurs when ρ is larger than 0.3. In contrast, the BER of enhanced TD-

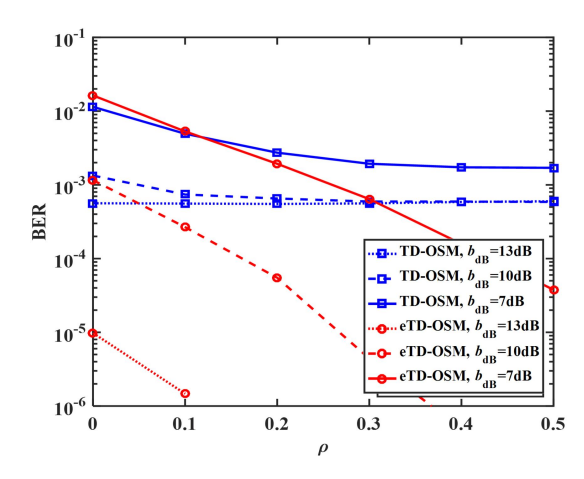


Fig. 4. BER vs. ρ for TD-SM and enhanced TD-SM (eTD-SM) for different DC bias levels with $N_t=4$ and a transmit SNR of 165 dB. The achieved spectral efficiency is 4 bits/s/Hz.

OSM is gradually reduced with the increase of ρ . Moreover, for a small DC bias of $b_{\rm dB}=7$ dB, TD-OSM performs better than enhanced TD-OSM when ρ is smaller than 0.1. However, enhanced TD-OSM achieves lower BER than TD-OSM when ρ is larger than 0.1. It can be seen that TD-OSM exhibits a BER floor of about 1.7×10^{-3} when ρ reaches 0.4, but enhanced TD-OSM can achieve further improved BER by applying a larger secondary DC bias. It can be concluded from Fig. 4 that enhanced TD-OSM is more sensitive to the adverse effect of zeros in the time-domain samples and can benefit from the addition of a relatively large secondary DC bias.

IV. CONCLUSION

In this paper, we have proposed and investigated a novel enhanced OFDM-based OSM scheme for bandlimited IM/DD OWC systems. The proposed enhanced OFDM-based OSM scheme can achieve substantially improved spectral efficiency while keeping moderate ICI and low transceiver complexity, when compared with the existing OFDM-based OSM schemes. To verify the superiority of the proposed enhanced OFDMbased OSM scheme over the existing ones, simulations have been conducted in a typical indoor 4×4 MIMO-OWC system. With a DC bias of 13 dB, it has been shown that enhanced OFDM-based OSM achieves a transmit SNR gain of 6.6 dB compared with conventional TD-OSM at a BER of 10^{-3} . When the DC bias is reduced, a proper secondary DC bias is required for both TD-OSM and enhanced OFDM-based OSM to mitigate the adverse effect of zeros in the time-domain samples. It has also been found that enhanced OFDM-based OSM achieves better BER performance when a relatively large secondary DC bias is added, making it very suitable for the application in OWC systems using visible light LEDs, i.e., visible light communication systems, where large DC biases are generally required to guarantee sufficient illumination.

REFERENCES

T. Cogalan and H. Haas, "Why would 5G need optical wireless communications?" in *Proc. IEEE Ann. Int. Symp. Pers., Indoor Mobile Radio Commun. (PIMRC)*, Oct. 2017, pp. 1–6.

- [2] Z. Ghassemlooy, S. Arnon, M. Uysal, Z. Xu, and J. Cheng, "Emerging optical wireless communications-advances and challenges," *IEEE J. Sel. Areas Commun.*, vol. 33, no. 9, pp. 1738–1749, Sep. 2015.
- [3] C. Chen, S. Fu, X. Jian, M. Liu, X. Deng, and Z. Ding, "NOMA for energy-efficient LiFi-enabled bidirectional IoT communication," *IEEE Trans. Commun.*, 2021. [Online]. Available: https://ieeexplore.ieee.org/document/9326355.
- [4] H. Elgala, R. Mesleh, and H. Haas, "Indoor optical wireless communication: potential and state-of-the-art," *IEEE Commun. Mag.*, vol. 49, no. 9, pp. 56–62, Sept. 2011.
- [5] S. Rajagopal, R. D. Roberts, and S.-K. Lim, "IEEE 802.15. 7 visible light communication: modulation schemes and dimming support," *IEEE Commun. Mag.*, vol. 50, no. 3, Mar. 2012.
- [6] R. Mesleh, H. Elgala, and H. Haas, "On the performance of different OFDM based optical wireless communication systems," J. Opt. Commun. Netw., vol. 3, no. 8, pp. 620–628, Aug. 2011.
- [7] T. Fath and H. Haas, "Performance comparison of MIMO techniques for optical wireless communications in indoor environments," *IEEE Trans. Commun.*, vol. 61, no. 2, pp. 733–742, Feb. 2013.
- [8] C. Chen, H. Yang, P. Du, W.-D. Zhong, A. Alphones, Y. Yang, and X. Deng, "User-centric MIMO techniques for indoor visible light communication systems," *IEEE Syst. J.*, vol. 14, no. 3, pp. 3202–3213, Sep. 2020.
- [9] M. Z. Afgani, H. Haas, H. Elgala, and D. Knipp, "Visible light communication using OFDM," in *Proc. Int. Conf. Testbeds Research Infrastructures Development Networks Communities (TRIDENTCOM)*, Mar. 2006, pp. 129–134.
- [10] D. Tsonev, H. Chun, S. Rajbhandari, J. J. McKendry, S. Videv, E. Gu, M. Haji, S. Watson, A. E. Kelly, G. Faulkner, M. Dawson, H. Haas, and D. O'Brien, "A 3-Gb/s single-LED OFDM-based wireless VLC link using a Gallium Nitride μLED," *IEEE Photon. Technol. Lett.*, vol. 26, no. 7, pp. 637–640, Apr. 2014.
- [11] C. Chen, W.-D. Zhong, and D. Wu, "Indoor OFDM visible light communications employing adaptive digital pre-frequency domain equalization," in *Proc. Conf. on Lasers and Electro-Optics (CLEO)*, Jun. 2016, paper JTh2A.118.
- [12] R. Mesleh, R. Mehmood, H. Elgala, and H. Haas, "Indoor MIMO optical wireless communication using spatial modulation," in *Proc. IEEE Int. Conf. Commun. (ICC)*, May 2010, pp. 1–5.
- [13] R. Mesleh, H. Elgala, and H. Haas, "Optical spatial modulation," J. Opt. Commun. Netw., vol. 3, no. 3, pp. 234–244, Mar. 2011.
- [14] X. Zhang, S. Dimitrov, S. Sinanovic, and H. Haas, "Optimal power allocation in spatial modulation OFDM for visible light communications," in *IEEE Veh. Technol. Conf. (VTC Spring)*, May 2012, pp. 1–5.
- [15] Y. Li, D. Tsonev, and H. Haas, "Non-DC-biased OFDM with optical spatial modulation," in *IEEE Int. Symp. Pers.*, *Indoor Mobile Radio Commun. (PIMRC)*, Sep. 2013, pp. 486–490.
- [16] P. Butala, H. Elgala, and T. D. Little, "Sample indexed spatial orthogonal frequency division multiplexing," *Chin. Opt. Lett.*, vol. 12, no. 9, p. 090602, Sep. 2014.
- [17] I. Tavakkolnia, A. Yesilkaya, and H. Haas, "OFDM-based spatial modulation for optical wireless communications," in *Proc. IEEE Globecom Workshops (GC Wkshps)*, Dec. 2018, pp. 1–6.
- [18] A. Yesilkaya, R. Bian, I. Tavakkolnia, and H. Haas, "OFDM-based optical spatial modulation," *IEEE J. Sel. Topics Signal Process.*, vol. 13, no. 6, pp. 1433–1444, Oct. 2019.
- [19] C. Chen, W.-D. Zhong, and D. Wu, "Communication coverage improvement of indoor SDM-VLC system using NHS-OFDM with a modified imaging receiver," in *Proc. IEEE Int. Conf. Commun. (ICC) Workshops*, May 2016, pp. 315–320.
- [20] C. Chen, W.-D. Zhong, and D. Wu, "Non-Hermitian symmetry orthogonal frequency division multiplexing for multiple-input multiple-output visible light communications," *J. Opt. Commun. Netw.*, vol. 9, no. 1, pp. 36–44, Jan. 2017.
- [21] A. Burton, H. Minh, Z. Ghassemlooy, E. Bentley, and C. Botella, "Experimental demonstration of 50-Mb/s visible light communications using 4× 4 MIMO," *IEEE Photon. Technol. Lett.*, vol. 26, no. 9, pp. 945–948, May 2014.
- [22] C. Chen, W.-D. Zhong, H. Yang, and P. Du, "On the performance of MIMO-NOMA-based visible light communication systems," *IEEE Photon. Technol. Lett.*, vol. 30, no. 4, pp. 307–310, Feb. 2018.